Elastic Properties of the Iron(II)–Triazole Spin Crossover Complexes [Fe(Htrz) 2 trz]BF 4 and [Fe(NH 2 trz) 3]SO 4

Damian Paliwoda, Laure Vendier, Livia Getzner, Frederico Alabarse, Davide Comboni, Baptiste Martin, Seyed Ehsan Alavi, Mario Piedrahita Bello, Lionel Salmon, William Nicolazzi, et al.

On the Elastic Properties of the Iron(II)-Triazole Spin Crossover Complexes $[Fe(Htrz)_2trz]BF_4$ and $[Fe(NH_2trz)_3]SO_4$

Damian Paliwoda,[#] Laure Vendier,[#] Livia Getzner,[#] Frederico Alabarse,[$] Davide Comboni,[&] Baptiste Martin,[#] Seyed Ehsan Alavi,[#] Mario Piedrahita Bello,[#] Lionel Salmon,[#] William Nicolazzi,[#] Gábor Molnár,[#] Azzedine Bousseksou[#]**

[#]LCC, CNRS & University of Toulouse, 205 route de Narbonne, 31077 Toulouse, France

[$]Elettra Sincrotrone Trieste, S.S. 14 - km 163,5 in AREA Science Park, 34149 Basovizza, Trieste, Italy

[&]ESRF, 71 Av. des Martyrs, 38043 Grenoble, France

ABSTRACT: Two benchmark Fe(II)-triazole spin-crossover (SCO) compounds, $[Fe(Htrz)_2trz]BF_4$ (**1**) and $[Fe(NH_2trz)_3]SO_4$ (**2**), have been investigated using variable temperature and pressure powder X-ray diffraction, dynamical mechanical analysis and differential scanning calorimetry techniques. We assessed the transformation strain, the compressibility and their anisotropy in both compounds. The measured bulk moduli are relatively high (20 and 13 GPa in **1** and **2**, respectively), but against expectations, the Fe-triazole chain direction is the most compressible crystal axis in **1**. We revealed considerable elastic softening and associated mechanical damping at the SCO in both compounds, which we interpreted, using the Landau theory, as a consequence of the coupling between the spin-state and the lattice strain. The magnitudes of the elastic potential energy (~15 %), stored elastic work (< 2-3 %) and frictional work (<3-4 %) with respect to the latent heat of the spin transition (26.8 and 19.5 kJ/mol in **1** and **2**, respectively) have been also assessed. The knowledge of these properties is important both for a better understanding of the SCO behavior of this important family of complexes as well as for guiding their integration into mechanical transducers and other technological applications.

1. INTRODUCTION

Certain (pseudo-)octahedral iron(II) complexes with N-donor ligands are known to undergo spin-crossover (SCO) phenomenon triggered by temperature, light irradiation, intense magnetic field, guest molecules and/or applied pressure.[1-4] This reversible switching between the paramagnetic high spin (HS) and diamagnetic low spin (LS) states is known to be strongly influenced by electron-lattice coupling, which often leads to cooperative behavior in the solid state, manifested notably by the emergence of first-order phase transitions with hysteresis loops. As a consequence of this bistability, switchable SCO molecules are very attractive and can potentially be used as components of memory devices, displays, sensors and actuators.[4-5]

Among the large variety of SCO compounds, one-dimensional, triazole-bridged iron(II) coordination polymers have received particular attention in the past decades.[7-12] These compounds of formulae $[Fe(4\text{-}R\text{-}1,2,4\text{-triazole})_3][anion]_2 \cdot nSolv$ (Solv = solvent molecules) consist of linear chains of ferrous ions linked by three N1,N2-1,2,4-triazole bridges. This short, rigid and stable linkage gives rise to unique properties with respect to other SCO compounds. First, its robustness provides a straightforward means to modify the triazole ligand at the 4-position (including even post-synthetic modifications[13]), providing access to a vast family of compounds.[7] This versatility is further enhanced by the possibility of counter-anion substitutions as well as the inclusion of solvent molecules. As such, the SCO properties can be tuned to a great extent, affording for Fe-triazole derivatives, which display SCO near and above room temperature.[7-18] Furthermore, the triazole bridge confers in many cases high cooperativity to these systems, manifested by large thermal hysteresis loops. These properties aroused tremendous interest since the pioneering works of Olivier Kahn for the technological use of this family of compounds.[19-20]

Due to notorious crystallization difficulties, most of the known triazole based iron(II) complexes are available only as polycrystalline materials, often of poor crystallinity. Despite the lack of single crystals, the chain type molecular structure of numerous iron-triazole complexes could be established very early using IR spectroscopy,[21] EXAFS (extended X-ray absorption fine structure)[22] and WAXS (wide angle X-ray scattering)[23] measurements as well as by comparison with analogous Cu(II)-triazole complexes,[24] providing suitable crystals for structural analysis. On this basis, it could be clearly established that in these compounds the iron(II) ion is surrounded by six triazole ligands, bridging it with two other metal ions and forming thus an infinite chain of iron-triazole units. More recently, a decisive progress could be achieved by solving the crystal structure of a few Fe(II) triazole complexes using either single-crystal X-ray diffraction[25-26] or powder X-ray diffraction (PXRD)[27-29] techniques. In particular, two complexes, $[Fe(NH_2trz)_3](NO_3)_2 \cdot nH_2O$[25] and $[Fe(NH_2trz)_3](BF_4)(SiF_6)_{0,5}$,[26] have been found suitable for detailed single crystal X-ray diffraction studies, though the former only in the LS state. The structural picture emerging from these efforts is nicely summarized in the PhD thesis of A. Grosjean.[26] Despite a relatively similar organization, based on parallel chains of $[Fe(R\text{-}trz)_3]_n$, these compounds can crystallize in various crystal systems (triclinic, orthorhombic, trigonal and hexagonal). The HS and LS phases are often isostructural, though the generalization of this point certainly requires further work. Remarkably, all these different structures display a common lattice parameter of ca. 7.3-7.9 Å (*c* in hexagonal and trigonal systems, *b* in orthorhombic and *a* in triclinic), which is just twice the distance between the nearest Fe ions in the chains. Importantly, in a given spin-state, this distance appears similar in each compound, resulting always in a similarly large variation of the corresponding lattice parameter (~5-6 %). The two other cell parameters, reflecting the inter-chain distances, display values of ca. 9-10 Å (or their multiples),

which depend in a subtle manner on the different inter-chain interactions involved (e.g. direct chain-chain or mediated by different anions and solvent molecules). Upon the LS to HS transition, these 'inter-chain lattice parameters' can display, however, strikingly different behaviors from one compound to other (e.g. increase, decrease or no change). It is worth noting also that the chains remain linear in the two spin states, but may exhibit relative movements (rotation/translation) among them.

This important progress in the structural analysis of Fe(II)-triazole chain complexes opens new prospects also for the investigation of the elastic properties of these compounds, which is the scope of the present paper. On one hand, the elasticity of the crystal lattice appears important, as it plays a key role in the cooperativity of the spin transition. Indeed, since the pioneering works of Spiering et al.[30-31] it is commonly accepted in the SCO community that the cooperativity of the SCO is governed primarily by short- and long-range elastic interactions, which arise due to the change of the size and shape of the molecules. Furthermore, the recent advances in the use of these Fe-triazole compounds in mechanical transducers (e.g. actuators,[32] sensors[33] and harvesters[34]) obviously calls for a better knowledge of their elastic properties.

Here, we focus on the compounds $[Fe(Htrz)_2trz]BF_4$ (**1**) and $[Fe(NH_3trz)_3]SO_4$ (**2**) (Figure 1), which were chosen for two main reasons. First, they are among the scarce Fe-triazole SCO complexes whose crystal structure has been solved in both spin states.[27-29] Second, both compounds exhibit remarkable behavior when undergoing SCO with relatively wide hysteresis loops above room temperature, coupled with a large volume change. These appealing features make them very attractive for various applications. In the present study, we have first confirmed and completed existing knowledge about the change of lattice parameters in the course of the thermal SCO for both compounds, which was followed by the investigation of the lattice

compressibility, using synchrotron PXRD under pressure. The temperature dependence of the elastic properties across the spin transition was then qualitatively assessed by means of dynamical mechanical analysis (DMA). Finally, the magnitude of elastic energy changes was evaluated in the context of differential scanning calorimetry (DSC) data, together with some other relevant thermodynamical properties.

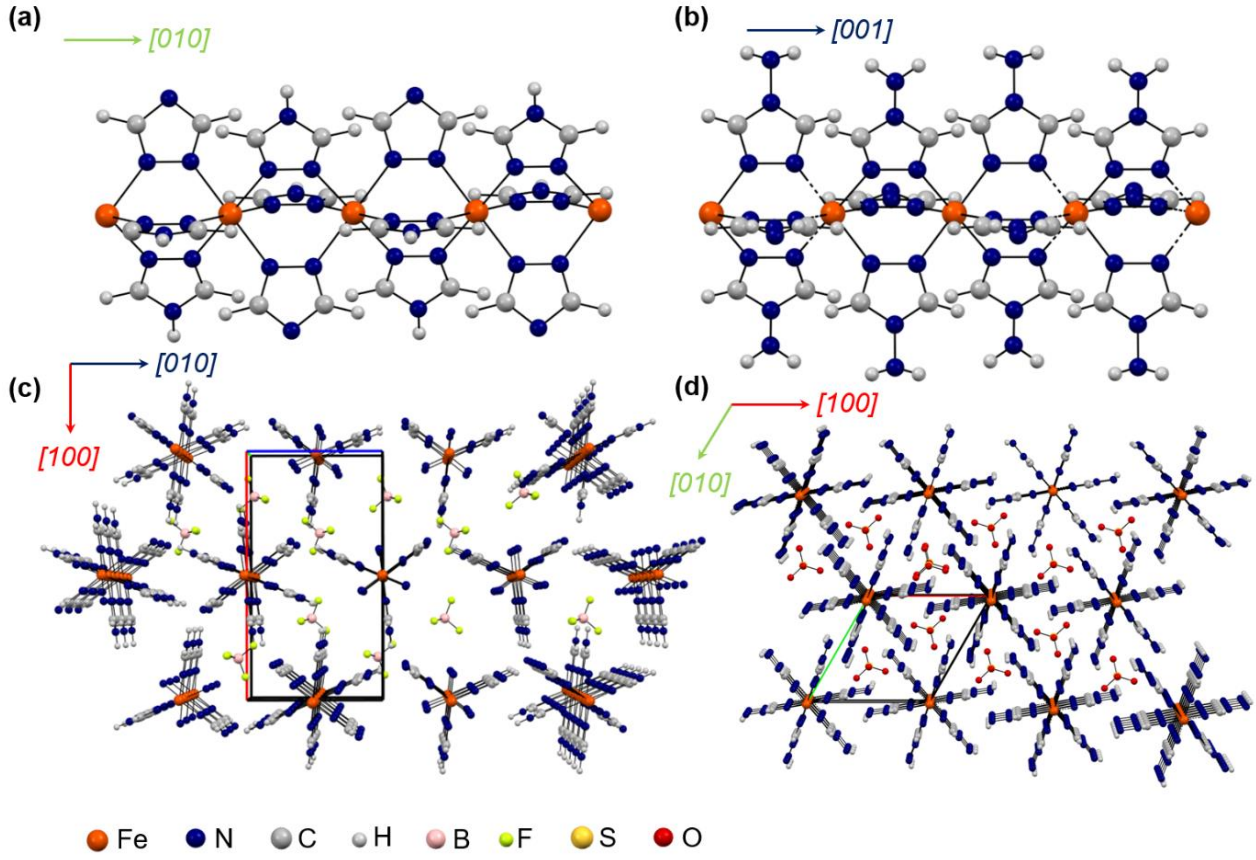

Figure 1. One-dimensional chains (a-b) and crystal packing (c-d) of the triazole-based iron(II) coordination polymers $[Fe(Htrz)_2trz]BF_4$ (a, c)[27] and $[Fe(NH_2trz)_3]SO_4$ (b, d).[28] Counter-ions have not been included in (a) and (b).

2. EXPERIMENTAL SECTION

2.1. Sample preparation. Polycrystalline samples of $[Fe(NH_2trz)_3]SO_4$ and $[Fe(Htrz)_2trz]BF_4$ were synthesized and characterized as described in previous reports.[35-36]

2.2. High-temperature PXRD. X-ray powder patterns were recorded on a Rigaku Smartlab instrument using a Cu source (λ = 1.54056 Å) and a fast linear detector (D Tex Ultra 250). The diffractometer was used in a theta/theta configuration with a "Cross Beam Optics" parabolic mirror in Bragg-Brentano mode, a 1 mm incident slit and a 20 mm receiving slit. Data were recorded in the 5 - 50° 2θ range (step: 0.02°, speed 1°/min), on heating and cooling between 20 – 140 °C, in ambient air, using as high temperature chamber the Rigaku XRD-DSC accessory.

2.3. High-pressure PXRD. High-pressure powder X-ray diffraction measurements were performed in two synchrotron X-ray facilities. $[Fe(NH_3trz)_3]SO_4$ was investigated both at the High Pressure Diffraction beamline, Xpress of the Elettra Sincrotrone Trieste (using PILATUS3 S 6M DECTRIS detector and an X-ray wavelength λ = 0.4955 Å) and on the ID15b beamline at the European Synchrotron Radiation Facility (using Eiger2XE 9M CdTe DECTRIS detector and an X-ray wavelength λ = 0.4104 Å). The latter beamline was also used to investigate the $[Fe(Htrz)_2trz]BF_4$ complex. Each sample was loaded separately into a membrane-driven diamond anvil cell together with a small ruby sphere and topped with Daphne 7373 oil.[37] The value of pressure was estimated before and after each XRD experiment from the shift in the R_1 fluorescence line of ruby.[38] In each case, the XRD images were converted to 1D diffraction profiles using Dioptas[39] and unit-cell parameters were refined using the LeBail[40] method, as implemented in the Jana2006 software. [41]

2.4. Dynamical mechanical analysis. DMA measurements were conducted between 10 and 130 °C at a heating/cooling rate of ±1 °C.min^{-1} by means of a DMA850 instrument (TA Instruments)

equipped with a special sample holder for powders.[42] The latter consists of two rectangular stainless steel pieces, among which the powder (ca. 50 mg) is disposed. The sample holder was mounted in a dual cantilever clamp and it was oscillated perpendicular to its base plane by a vertical motion of the middle clamp (see Fig. 2 and Scheme S1 in the Supporting Information, SI). The measurements were conducted in constant strain mode with 0.08 % strain amplitude at different frequencies (1, 10 and 100 Hz). Each sample was measured through several thermal cycles to verify the reproducibility of the results. Owing to the powdery nature of the samples, absolute values of storage and loss moduli (*E'* and *E''*) cannot be reliably assessed, but their variation provides relevant information on thermally induced changes of viscoelastic properties.

2.5. Differential scanning calorimetry. DSC thermograms were acquired using a Netzsch DSC 3500 Syrius instrument with a heating/cooling ramp of ±10 °C/min and a nitrogen gas purge of 20 mL/min. The samples were placed in a standard aluminum sample pan. Temperature and enthalpy were calibrated using the melting transition of indium.

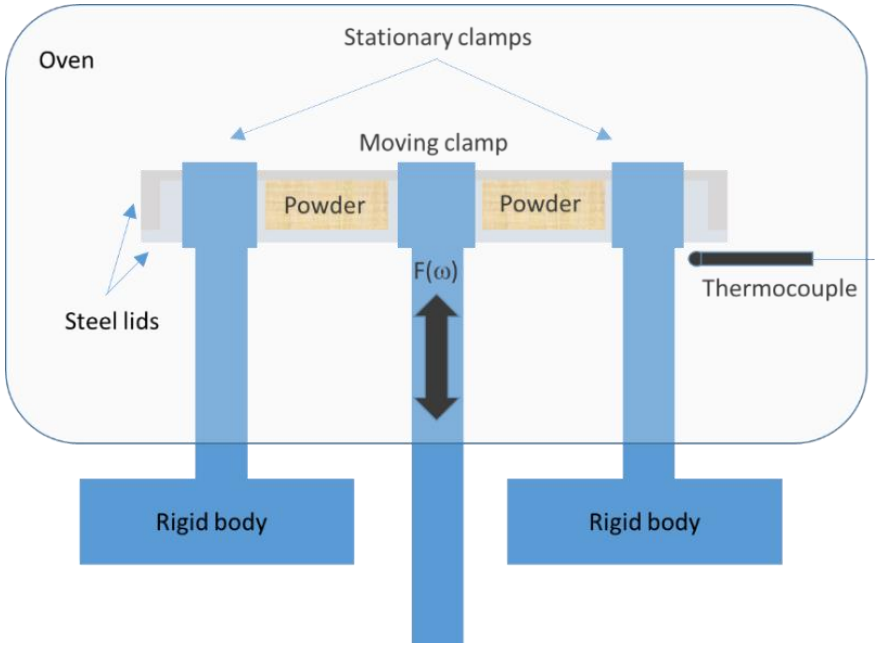

Figure 2. Scheme of the DMA setup using a dual cantilever clamp with a powder sample holder

3. RESULTS AND DISCUSSION

3.1. Thermal strain of the crystal lattice. The HS and LS crystal structures of $[Fe(Htrz)_2(trz)](BF_4)$ (**1**) were determined and refined at 420 K and 300 K by Grosjean et al.[27] Compound **1** forms orthorhombic crystals, space group *Pnma*, in which the iron(II) ion lies on an inversion center and is coordinated by two Htrz and one trz bridging ligands (see Fig. 1a and 1c). The structure of the compound $[Fe(NH_2trz)_3]SO_4$ (**2**) was assessed in the LS state by Sirenko et al.[28] and completed later with the HS state structure by Nieto-Castro[29]. Compound **2** crystallizes in the hexagonal $P6_3/m$ space group with two formula units per cell. Similar to complex **1**, the iron(II) ion is coordinated by six NH_2-trz ligands bridging the neighboring metal centers (see Fig. 1b and 1d). Both structures are based on short intermolecular interactions between positively charged iron(II)-triazole chains and counter-anions. The packing of **1** is mostly governed by N-$H_{(H\text{-}triazole)}\cdots N_{(triazole)}$ interchain hydrogen bonds and $CH_{(triazole)}\cdots F_{(anion)}$ anion-chain interactions, while in compound **2** the anion-chain interactions become even stronger. This is due to the bulkier ligand obtained by the introduction of the NH_2- group on the triazole moiety. Nevertheless, the amino group is also involved in the formation of inter-chain interactions. Besides, each $[Fe(NH_2trz)_3]_n$ chain is connected with the sulphate ion *via* N-$H_{(amino\text{-}group)}\cdots$O hydrogen bonds and short SO_4 anion$\cdots\pi$(triazole ligand) interactions.

We have performed a series of variable temperature PXRD experiments on both polycrystalline samples. Representative diffractograms in the two spin states are shown in Figure 3 and the main structural parameters are summarized in Table 1 (see Figures S1-S4 for a compilation of the ensemble of the experimental data). In the case of **1**, a detailed variable-temperature PXRD analysis has been already reported by Grosjean et al.[26-27] and for this compound, our objective was thus merely to confirm if the sample in our hands displays the same

behavior. However, no detailed temperature dependence was published for compound **2** and we report here the analysis of thermal strain in this material. As expected, at high temperatures, both complexes undergo a reversible transition from the LS to the HS form, accompanied with a large expansion of the unit cell volume (Figure 4a). Compound **1** expands its volume by nearly 11 %, the initially denser **2** only by 5 %. It is interesting to remark that the ordinary thermal dilation of the two compounds is rather small in all crystallographic directions and in both spin-states (see Fig. 4 and Fig. S5), characterized by linear thermal expansion coefficients of the order of 10^{-5} K^{-1}. The origin of this phenomenon requires further investigations, but it is worth to remark that zero or even negative thermal expansion is relatively frequent in network structures,[43] and we can thus tentatively suggest that this might be a recurrent feature in Fe(II)-triazole chains as well.

Table 1. PXRD-derived unit-cell parameters obtained for polycrystalline forms of compounds **1** and **2** in the two spin states.

Compound	$[Fe(Htrz)_2(trz)]BF_4$ (**1**)		$[Fe(NH_2trz)_3]SO_4$ (**2**)	
Molecular weight (g/mol)	348.8		407.1	
Spin state	LS	HS	LS	HS
Temperature (°C)	44	129	24	109
Space group, *Z*	*Pnma*, 4	*Pnma*, 4	$P6_3/m$, 2	$P6_3/m$, 2
a (Å)	17.24(1)	17.32(3)	10.071(1)	10.05(1)
b (Å)	7.353(8)	7.89(2)	10.071(1)	10.05(1)
c(Å)	9.165(8)	9.49(2)	7.378(1)	7.75(1)
α, β, γ (°)	90, 90, 90	90, 90, 90	90, 90, 120	90, 90, 120
V ($Å^3$)	1161(2)	1296(4)	648.03(17)	678(2)
d (g/cm^3)	1.995	1.788	2.086	1.994

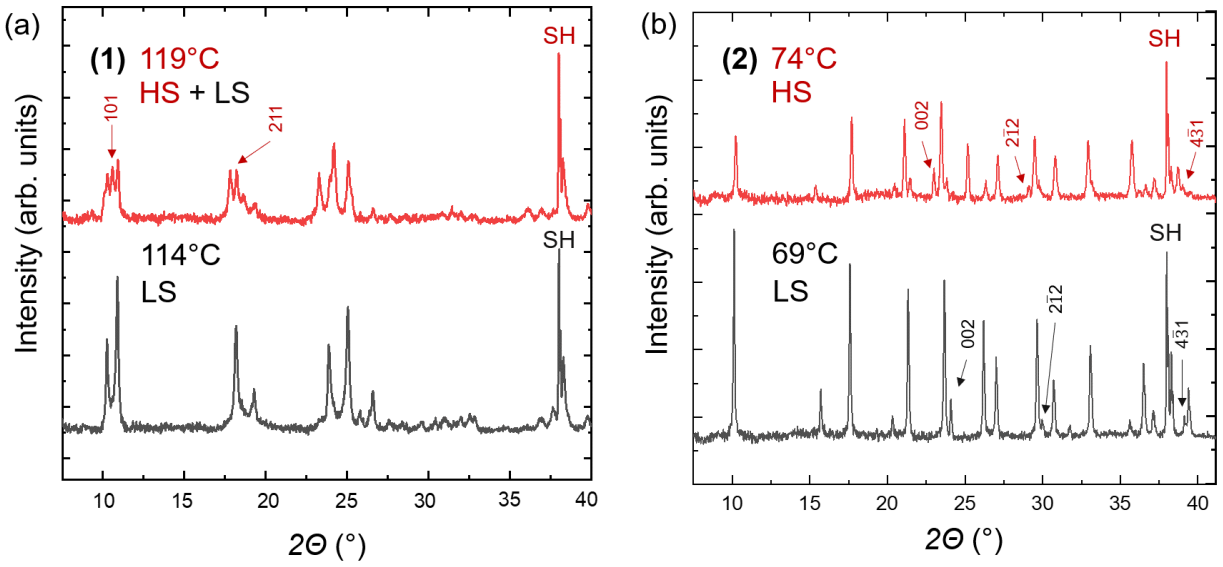

Figure 3. Representative PXRD patterns of complexes **1** (a) and **2** (b) in the LS and HS states. Selected SCO marker peaks are highlighted. SH indicates signal from the sample holder.

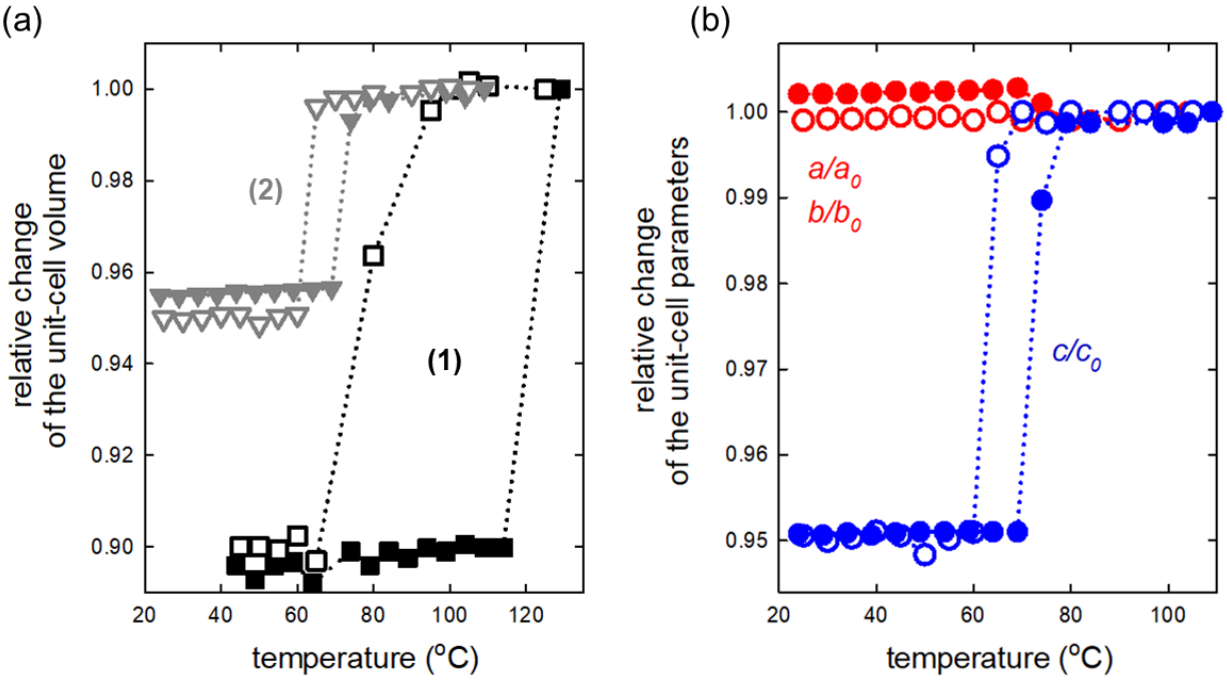

Figure 4. Thermal expansion of the complexes: (a) comparison of the relative volume change in **1** and **2** showing wide hysteresis loops, and (b) relative change of the unit cell parameters of compound **2**. (Filled/empty symbols represent heating/cooling.)

Importantly, highly anisotropic transformation strains have been found in both complexes. The largest strain contribution occurs always in the direction of the chains: 6.5 % expansion along parameter *b* in the tetrafluoroborate derivative and 5.0 % along parameter *c* in the sulfate salt. On the other hand, the other cell parameters display dissimilar behavior. In compound **1**, the strain is considerable in the *c* (3.5 %) and *a* (0.5 %) directions, whereas no sizeable strain was observed in the *a* (= *b*) crystallographic direction in compound **2**. (*N. B.* A slight, irreversible variation of parameter *a* was observed upon the first heating, most likely due to a loss of residual solvents.)

3.2. Compressibility and pressure-induced lattice transformations. Three series of high-pressure PXRD measurements have been performed at room temperature on our samples using synchrotron X-ray sources. Compounds **1** and **2** were compressed up to 3.2 GPa in the LS forms at ID15b of the European Synchrotron Radiation Facility, and a further run was conducted up to 5 GPa for compound **2** at Elettra Sincrotrone Trieste. LeBail refinements have been performed for each diffractogram in order to extract the unit-cell parameters, which are reported in the SI (see Figures S6-S11 and Tables S1-S7). Both complexes show monotonic compressibility, although highly anisotropic behavior of unit-cell parameters has been revealed (Fig. 5). Third order Birch–Murnaghan equations of state were roughly fitted to the unit cell volume evolution of **1** and **2** with pressure using EosFit7.[44] The bulk modulus of **1** in the LS state is equal to 20 (±3) GPa, which is exceptionally high among other SCO complexes displaying values typically in the range between 5-12 GPa.[45] Such low compressibility, combined with a large volume change at the SCO should explain the outstanding cooperativity of this compound. Against odds, the most compressive direction turns out to be the *b*-axis, along the chains. This unexpected finding stems likely from the compact lattice packing of **1**, characterized by short inter-chain distances. Interestingly, a

negative linear compressibility of parameter *a* is observed between ca. 2.2 and 3.5 GPa in this compound, which may suggest the rearrangement of the chain – anion interactions.

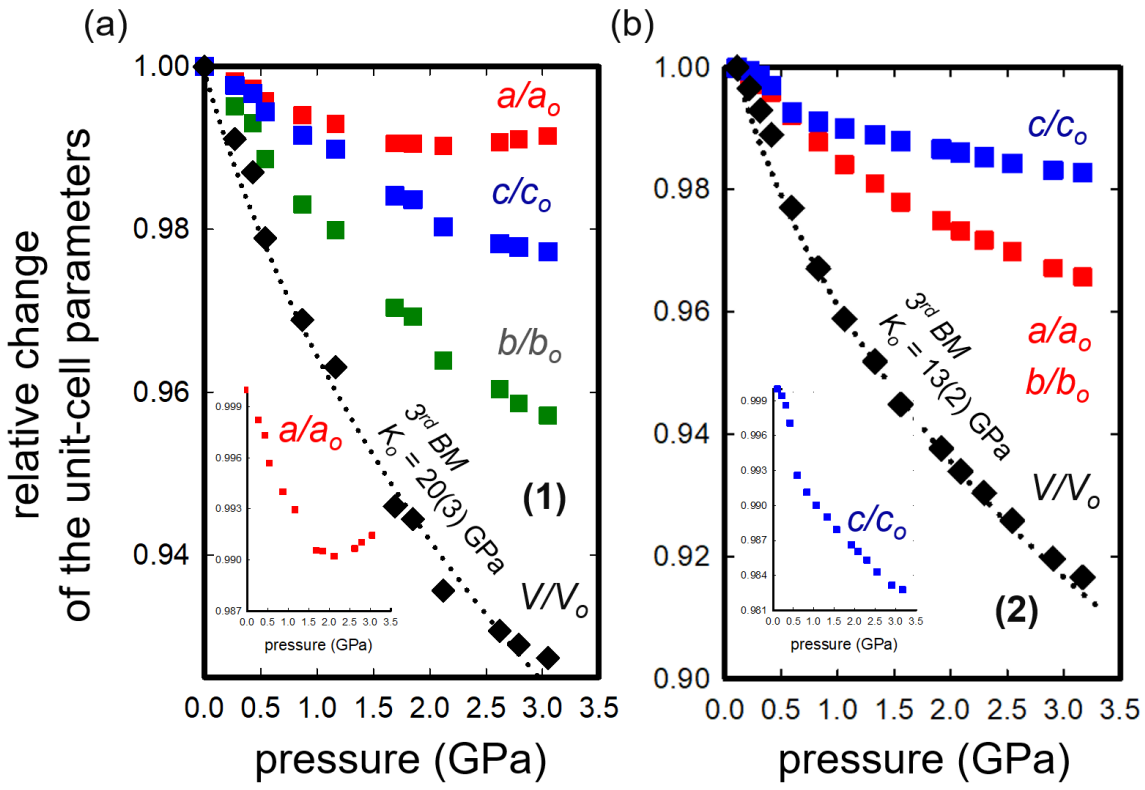

Figure 5. Pressure-induced unit cell transformations of complexes **1** (a) and **2** (b). Dotted lines show the fits for the bulk moduli. The insets show anomalies detected in the compressibility of the unit-cell parameters: negative linear compressibility of parameter *a* above 2.2 GPa in complex **1** and the drop of parameter *c* around 0.7 GPa in complex **2**.

The bulk modulus of **2** is significantly lower, ca. 13 (±2) GPa, but can be considered still high in comparison with other SCO systems.[45] In contrast to **1**, where the most compressible unit-cell parameter is the one along the chains, complex **2** manifests the opposite behavior with the parameter *c* being the least compressible. One must note, however, that an anomalous behavior of

parameter *c* has been detected between ca. 0.59 and 0.83 GPa, which was also confirmed in a second series of experiments performed at Elettra Sincrotrone Trieste. This discontinuity suggests the occurrence of a structural transition, which should be confirmed by structural refinements (out of the scope of the present paper). We just note here that in the low-pressure range (< 0.6 GPa) the compressibility of **2** seems actually fairly isotropic (within the experimental uncertainties).

3.3. Dynamical mechanical analysis. Besides the room temperature elastic moduli, the temperature dependence of elastic properties across the spin transition is of considerable interest as well. To investigate this question, we conducted variable temperature DMA measurements. In general, DMA tests require 'compact', freestanding samples (e.g. pellets, films, large crystals), which can be investigated in tension, compression, bending or shear configurations. However, the SCO phenomenon is notoriously sensitive to mechanical treatments and pelletizing does not appear as a good option.[1] Another possibility is to embed the SCO particles in a suitable matrix, enabling to fix the geometry of the sample as a composite film. This strategy is more promising, but the extraction of the particle viscoelastic properties is not straightforward and the matrix might also affect the SCO properties of the particles.[4] We have thus decided to analyze directly the neat polycrystalline samples. At this point, it is important to underline that the complex dynamical moduli obtained from DMA on such loose powder samples remains only a qualitative measure of their viscoelastic behaviors. In particular, the magnitude of the storage modulus (*E'*) is dominated by the steel sample holder (see Fig. 1) and its absolute value cannot be easily interpreted. On the other hand, since steel behaves elastically in the temperature range of our interest, any step transition of *E'* or peak in the loss tangent ($\tan\delta$) should be interpreted as a thermally induced phenomenon in the powder sample. Indeed, this approach has been successfully used in the past to investigate glass and melting transitions in various powder samples.[42,46-48]

Representative data for E' and tanδ, recorded on heating and cooling are shown in Figure 6 for our two powder samples (see also Figures S12-S13 in the SI). For both samples, tanδ exhibits distinct peaks at the spin transition, which indicates, as it can be expected,[49-50] enhanced internal frictions in the course of the spin transition.

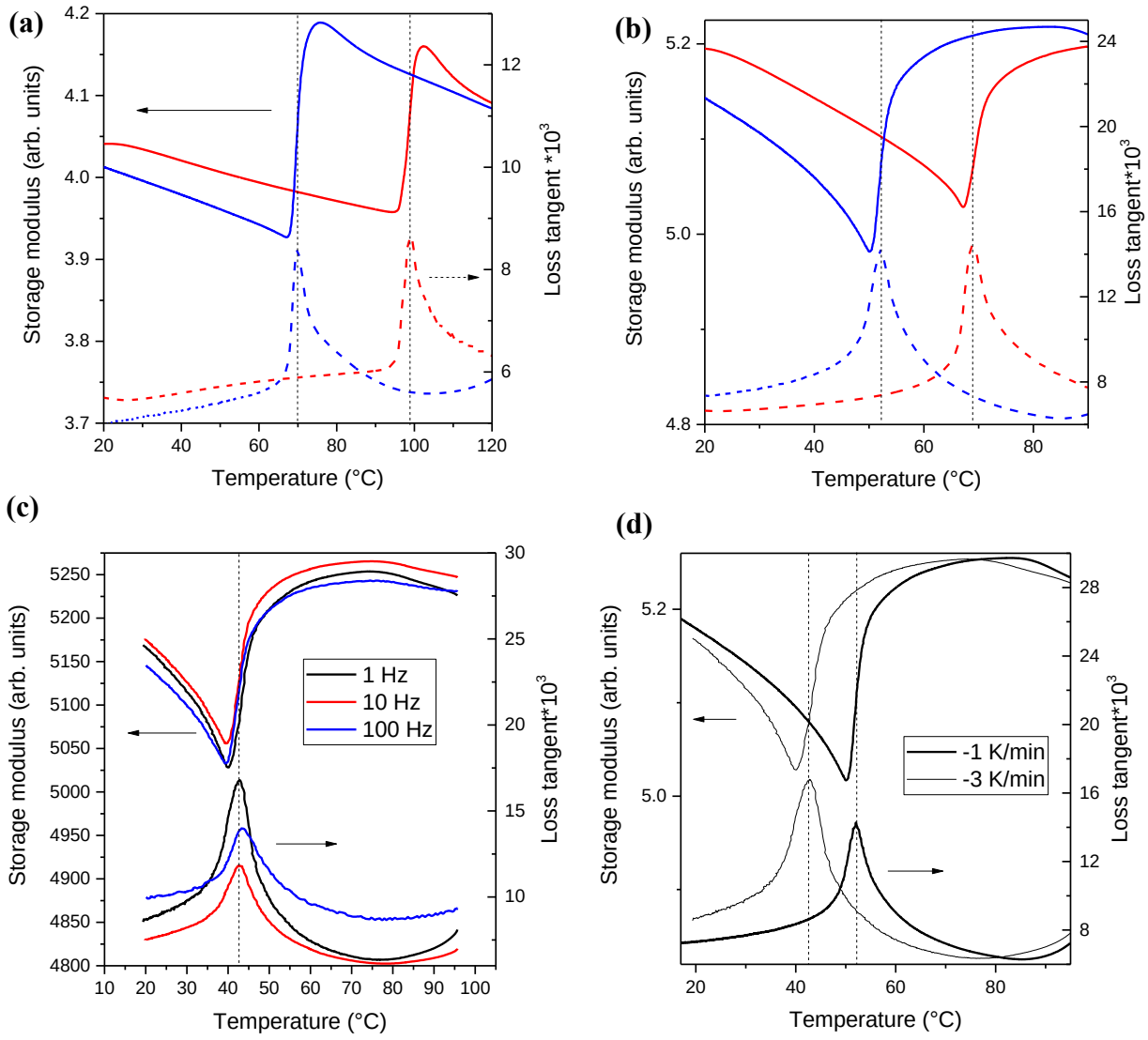

Figure 6. Temperature dependence of the storage modulus and loss tangent for **1** (a) and **2** (b) acquired upon heating (red) and cooling (blue). Storage modulus and loss tangent recorded for **2** in the cooling mode at selected oscillation frequencies (c) and cooling rates (d). The vertical dashed lines show the spin transition temperatures.

At a first glance, the temperature dependence of the storage modulus of sample **1** exhibits a reversible increase when going from the LS to the HS state (Fig. 6a) – in close resemblance with our previous DMA measurements on polymer composite films containing particles of **1**.[51] In the case of the composite samples, we argued that the counter-intuitive increase of the stiffness in the HS phase might arise from the increase of the particle volume fraction in the composite material. The present results on the neat powder sample clearly invalidate our previous hypothesis. Nonetheless, a stiffening of the particles in the less dense HS phase appears unphysical. A first explanation for this apparent discrepancy comes from the DMA analysis of sample **2** (Fig. 6b), which points more clearly to the existence of a dip of *E'* around the spin transition temperature – instead of a step-like change. In other words, the elastic modulus changes observed in our experiments do not reflect the difference of the 'normal' stiffness of the two phases. Instead, they arise due to the spin transition itself. Similar to other types of phase transitions,[52] and in-line with previously reported resonant ultrasonic spectroscopy measurements on a few molecular SCO compounds[53-55] and static compression of iron-bearing minerals,[56] we therefore suggest that the elastic softening at the spin transition observed in our experiments should be induced by the coupling of the spin-state of the molecules to lattice strains. Indeed, when an SCO material is subjected to an external stress, as in a DMA experiment, it will deform to some extent, which depends on its elastic constants. However, a change in the strain state of the material will result in a change of the HS-LS equilibrium, because it affects the free energy of the HS and LS phases unequally. Specifically, tensile strains will favor the HS form, which has higher volume, whereas compression has the opposite effect. The material will thus adjust its spin state in response to the applied external stress until new equilibrium is reached. The spin-state of the system provides thus an additional, indirect and time-dependent (anelastic) link between stress and strain, in addition to

the ordinary instantaneous (elastic) response.[57] This relaxation of the spin state of the system acts to facilitate the deformation, because the SCO also contributes to the change of strain state. Hence, the material appears effectively softer than it would be in the absence of this relaxation. In addition, since the relaxation process is irreversible, energy is dissipated and there will be thus a phase lag between stress and strain, which depends on the relaxation time of the system and the frequency of the applied stress. Cases in which the SCO occurs via phase separation, i.e. first-order transitions, offer more complications due to the fact that the applied stress may move the HS/LS interface(s), in addition to changing the local equilibrium of the system. Further, when the SCO crystallite is embedded in a matrix of other particles, other damping mechanisms might arise, such as grain boundary relaxation.[57]

Before moving to a more formal analysis of this elastic softening phenomenon, we shall discuss our experimental observations regarding the mechanical loss behavior, seen as peaks of $\tan\delta$ at the spin transition (Fig. 6). These loss peaks do not exhibit the same large asymmetry as the storage modulus patterns and they coincide with the point of the largest slope in the $E'(T)$ curve (indicated by dashed vertical lines in Fig. 6). This point should correspond thus to the spin transition temperature, where the spin state of the material is the most sensitive to any change of external stress. Further, variable frequency (1-100 Hz) and variable temperature rate (1-3 K/min) DMA measurements revealed that the amplitude of mechanical loss peaks are clearly reduced at increasing frequencies and lower scan rates (Fig. 6c-6d), which was reproducibly observed in our experiments. Importantly, one should also notice that the loss peaks do not shift with changing frequency, something unusual for a relaxation process, but it is actually a general feature of anelastic relaxations, which arise due to phase transitions.[57] One might wonder that besides the spin-state relaxation, which is thought to govern the elastic softening, some additional damping

mechanisms might exist. Indeed, such low-frequency (~1 Hz) mechanical responses at first-order phase transitions are usually associated with interfacial phenomena,[57] which could be internal frictions at HS/LS phase boundaries in our case. Nevertheless, it is worth mentioning that pronounced loss peaks at the SCO were reported previously at much higher frequencies in resonant ultrasound spectroscopy experiments[53-55] (~1 MHz) and MEMS based measurements[58] (~50 kHz) even for materials displaying continuous transitions, for which no phase separation is expected. Further investigations over a broad range of frequencies and temperatures will be thus indispensable to properly 'map' the anelastic response of SCO materials.[59]

As discussed in detail by Carpenter and Salje,[52] to calculate the elastic constant variations at a phase transition, the excess Gibbs free energy ΔG_{excess} can be written in terms of a Landau potential, $L(\eta)$, the elastic strain energy, $\Delta G_e(\varepsilon)$, and the coupling energy, $\Delta G_c(\eta, \varepsilon)$, as:

$$\Delta G_{excess} = L(\eta) + \Delta G_c(\eta, \varepsilon) + \Delta G_e(\varepsilon) = L(\eta) + \sum_{i,m,n} \lambda_{i,m,n} \varepsilon_i^m \eta^n + \frac{1}{2} \sum_{ij} C_{ij}^{\circ} \varepsilon_i \varepsilon_j \qquad \text{(Eq. 1)}$$

The first term $L(\eta)$ accounts for the contributions from the order parameter η alone. The second term describes the interaction between the order parameter and the transformation strains ε_i (in Voigt notation), where $\lambda_{i,m,n}$ is the strain - order parameter coupling coefficient. Finally, the last term accounts for the elastic energy, where C_{ij}° are the relevant elastic constants of the high-symmetry phase. The exponents *m* and *n* depend on the symmetry properties of η and ε. In the case of an isostructural spin transition, the 'Landau term' can be written, as discussed by Chernyshov[60] and Collet[61-62], as:

$$L(\eta) = A\eta_{spin} + \frac{1}{2} B {\eta_{spin}}^2 + \frac{1}{4} C {\eta_{spin}}^4 \qquad \text{(Eq. 2)}$$

where $A = a(T_{SCO} - T)$, *B* and *C* are the phenomenological parameters of the Landau potential, and η_{spin}, the totally symmetric order parameter, is given by the number *N* of HS and LS molecules (or, alternatively, by the fraction of LS molecules n_{LS}) as:

$$\eta_{spin} = \frac{N_{HS}-N_{LS}}{N_{HS}+N_{LS}} = 1 - 2n_{LS} \qquad \text{(Eq. 3)}$$

η_{spin} transforms as the identity representation and takes values between -1 (LS) and +1 (HS). In the following, let us consider the case of compound **2** with a hexagonal $P6_3/m$ structure, for which symmetry, the combination of Equations 1 and 2 gives:

$$\Delta G_{excess} = A\eta_{spin} + \frac{1}{2}B{\eta_{spin}}^2 + \frac{1}{4}C{\eta_{spin}}^4 + \lambda_1 n_{LS}(\varepsilon_1 + \varepsilon_2) + \lambda_2 n_{LS}\varepsilon_3 + \lambda_3 n_{LS}({\varepsilon_4}^2 + {\varepsilon_5}^2) +$$

$$+\lambda_4 n_{LS}[{\varepsilon_6}^2 + (\varepsilon_1 - \varepsilon_2)^2] + \frac{1}{4}(C_{11}^{\circ} + C_{12}^{\circ})(\varepsilon_1 + \varepsilon_2)^2 + \frac{1}{4}(C_{11}^{\circ} - C_{12}^{\circ})(\varepsilon_1 - \varepsilon_2)^2 + C_{13}^{\circ}(\varepsilon_1 +$$

$$\varepsilon_2)\varepsilon_3 + \frac{1}{2}C_{33}^{\circ}{\varepsilon_3}^2 + \frac{1}{2}C_{44}^{\circ}({\varepsilon_4}^2 + {\varepsilon_5}^2) + \frac{1}{2}C_{66}^{\circ}{\varepsilon_6}^2 \qquad \text{(Eq. 4)}$$

As a first approximation, only the lowest order symmetry-allowed couplings are considered in Equation 4, which are bilinear for the non-symmetry-breaking strains (ε_1=$\varepsilon_2, \varepsilon_3$) and linear-quadratic for the symmetry-breaking strains ($\varepsilon_4 = \varepsilon_5 = \varepsilon_6 = 0$). To derive the temperature dependence of the elastic constants C_{ij}, for which $i,j = 1-3$, one can conveniently use the formula:[52]

$$C_{ij} = C_{ij}^{\circ} - \frac{\partial^2 G}{\partial \varepsilon_i \partial n_{LS}} \chi \frac{\partial^2 G}{\partial n_{LS} \partial \varepsilon_j} \qquad \text{(Eq. 5)}$$

wherein the so-called order parameter susceptibility, χ, is given by:

$$\chi = \left(\frac{\partial^2 L}{\partial {\eta_{spin}}^2}\right)^{-1} = \frac{1}{B + 3C{\eta_{spin}}^2} \qquad \text{(Eq. 6)}$$

Applying equation 5 on equation 4, one obtains the following variations of elastic constants:

$$C_{11} = C_{22} = C_{11}^{\circ} - {\lambda_1}^2\chi \qquad \text{(Eq. 7a)}$$

$$C_{33} = C_{33}^{\circ} - {\lambda_2}^2 \chi \quad \text{(Eq. 7b)}$$

$$C_{12} = C_{12}^{\circ} - {\lambda_1}^2 \chi - 2\lambda_4 n_{LS} \quad \text{(Eq. 7c)}$$

$$C_{13} = C_{23} = C_{13}^{\circ} - \lambda_1 \lambda_2 \chi \quad \text{(Eq. 7d)}$$

The remaining elastic constants are obtained as:

$$C_{44} = C_{55} = \frac{\partial^2 G}{\partial {\varepsilon_4}^2} = C_{44}^{\circ} + 2\lambda_3 n_{LS} \quad \text{(Eq. 9)}$$

$$C_{66} = \frac{\partial^2 G}{\partial {\varepsilon_4}^2} = C_{66}^{\circ} + 2\lambda_4 n_{LS} = \frac{1}{2}(C_{11} - C_{12}) \text{ (Eq. 10)}$$

The shear modulus, determined primarily by the behaviors of C_{44} and C_{66}, is therefore expected to show a stepwise evolution, mirroring the behavior of $n_{LS}(T)$. On the other hand, the bulk modulus behavior is dictated by the evolution of C_{11}, C_{12}, C_{13} and C_{33}. Indeed, equations 7a-7d predict a classical elastic softening behavior of the bulk modulus of **2**, wherein the variation of the relevant elastic constants, ΔC_{ij}, is proportional to the square of the elastic coupling strength, λ^2 and the order parameter susceptibility, χ (i.e. the shape of the Landau potential).[52]

At this stage, it is important to remark that the storage modulus measured by DMA on our loose powder samples should contain contributions from both the shear and the bulk moduli of the particles, but in a way, which is difficult to predict by computations. As such, the experiments reflect only in a qualitative manner the softening of certain elastic constants at the spin transition, which is predicted by theory. For a quantitative link, further experiments on single crystal samples will be indispensable.

3.4. Calorimetric analysis. Since the pioneering works of Sorai and Seki,[63-64] calorimetric techniques have been extensively used to investigate the enthalpy and entropy changes associated with the SCO phenomenon. Particular attention is devoted to the analysis of vibrational entropy changes, which are considered as the main driving force of the thermally induced SCO.[65-66]

However, in analogy with the martensitic transition in shape memory alloys,[67-70] it appears interesting to discuss the calorimetric data with respect to the various thermo-elastic phenomena taking place in SCO materials.

Figure 7 shows the DSC curves acquired for samples **1** and **2** on five successive heating-cooling cycles. For compound **2**, the DSC peaks associated with the SCO are perfectly reproducible following the first run-in cycle with standard-deviations of the peak positions and areas inferior to 0.3 %, whereas for compound **1** the same level of reproducibility is reached only after the second thermal cycle. The characteristic transformation temperatures and the measured heat exchange (q_{DSC}) during the transitions are tabulated in Tables S8-S9 (see the SI).

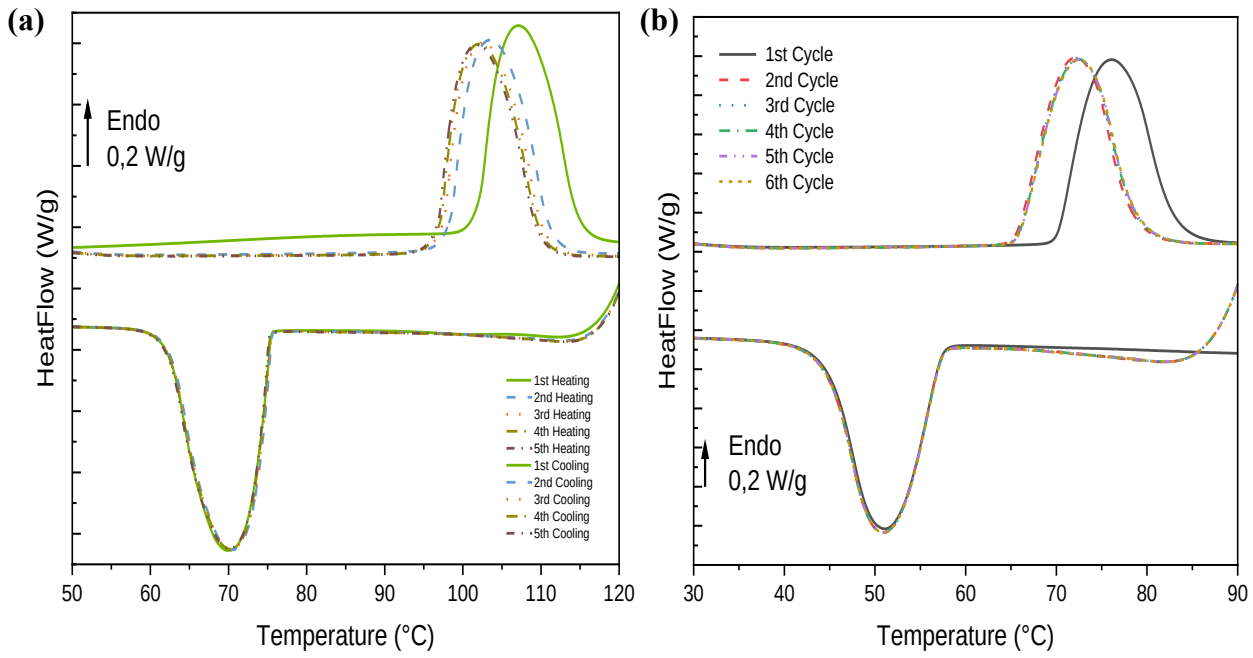

Figure 7. DSC thermograms of powder samples of **1** (a) and **2** (b) acquired upon heating and cooling for five successive thermal cycles.

To a first approximation, the mean value of the exchanged heat upon the forward (HS→LS) and reverse (LS→HS) transitions can be considered equal to the transformation enthalpy:

$$\frac{q_{DSC}^{\mathrm{LS}\rightarrow\mathrm{HS}} - q_{DSC}^{\mathrm{HS}\rightarrow\mathrm{LS}}}{2} \approx \Delta H_{SCO} = H_{HS} - H_{LS} = T_{eq}\Delta S_{SCO} \qquad \text{(Eq. 10)}$$

wherein the equilibrium temperature ($\Delta G_{SCO}(T_{eq}) = 0$) is roughly approximated by:

$$T_{eq} \approx \frac{T_{SCO}^{\mathrm{LS}\rightarrow\mathrm{HS}} + T_{SCO}^{\mathrm{HS}\rightarrow\mathrm{LS}}}{2} \qquad \text{(Eq. 11)}$$

Neglecting rotational and configurational degrees of freedom, the vibrational entropy can then be calculated as a difference of the total entropy change and electronic entropy change - taking only the spin multiplicity ratio ($\frac{5}{1}$) of the HS and LS states of the ferrous ions:[63]

$$\Delta S_{SCO}{}^{vib} = \Delta S_{SCO} - \Delta S_{SCO}{}^{spin} \approx \frac{\Delta H_{SCO}}{T_{eq}} - Rln(\frac{5}{1}) \qquad \text{(Eq. 12)}$$

Table 2 summarizes the calculated data for the two compounds, which are found in good agreement with previous reports.[28] In particular, one can note the significant vibrational entropy contribution (*ca.* 80 %), which provides the main driving force for the thermal spin transition in these materials.

Table 2. Thermodynamical parameters extracted from DSC measurements for samples **1** and **2**

Sample	ΔH_{SCO} kJ/mol	ΔG_{ε} kJ/mol	ΔS_{SCO} J/(K.mol)	$\Delta S_{SCO}{}^{vib}$ J/(K.mol)	W_f kJ/mol	W_{el} kJ/mol	ΔC_p J/(Kmol)
1	26.8	-	74.6	61.2	≤ 1.2	≤ 0.5	~18
2	19.5	~3	58.2	44.8	≤ 0.6	≤ 0.4	~6

Another interesting parameter we can extract from our experimental data is the elastic potential energy (ΔG_{ε}) contribution to the latent heat. In compound **2**, the spontaneous strain of the spin transition contains only one component, namely, ε_3. The elastic energy contribution can be therefore calculated simply by:

$$\Delta G_{\varepsilon} = \frac{1}{2} C_{33}^{\circ} {\varepsilon_3}^2 \qquad \text{(Eq. 13)}$$

From the data in Fig. 5b, the elastic constant C_{33}° can be roughly estimated comparable with the bulk modulus (*ca.* 13 GPa), giving $\Delta G_{\varepsilon} \approx 3\ \mathrm{kJ/mol}$, i.e. ~15 % of the latent heat. It seems likely that this contribution is even higher in compound **1**, which is not only sizably stiffer, but displays much higher strain contributions as well.

Another useful way to analyze the calorimetric data is based on the distinction between chemical and non-chemical energies that drive the transition.[67-70] The main driving force for the spin transition is the chemical free energy difference (ΔG_{chem}) between the HS and LS phases:

$$\Delta G_{chem} = \Delta H_{SCO} - T\Delta S_{SCO} = (T - T_{eq})\Delta S_{SCO} \qquad \text{(Eq. 14)}$$

However, the fact that the heat of transformation is exchanged with the surroundings at different temperatures ($T_{SCO}^{\mathrm{LS}\rightarrow\mathrm{HS}}$ and $T_{SCO}^{\mathrm{HS}\rightarrow\mathrm{LS}}$) is responsible for entropy production, since the same amount of heat absorbed at high temperature is released then at a lower temperature. An irreversible thermodynamical work, coined in the literature as 'frictional work', W_f, , must be thus involved in the transition process, which opposes both the forward and reverse transformations and is therefore responsible for the entropy production.[67] The actual operative mechanisms of this dissipation phenomenon (*sic* 'hysteresis loss') are not known for SCO materials, but in analogy with other phase change materials it should be related to interfacial phenomena and might also involve the emission of acoustic waves.[71] Nevertheless, even without the knowledge of the exact mechanisms, the thermodynamics frame can be discussed. The frictional work consumes the available driving force, and therefore the chemical free energy represents, according to the second law of thermodynamics, an upper limit to W_f such as:[67]

$$\Delta G = (T_{tr} - T_{eq})\Delta S_{SCO} \geq W_f \qquad \text{(Eq. 15)}$$

where $T_{tr} = T_{SCO}^{\mathrm{HS}\rightarrow\mathrm{LS}}$ and $T_{tr} = T_{SCO}^{\mathrm{LS}\rightarrow\mathrm{HS}}$ for the forward and reverse transitions, respectively. For compounds **1** and **2** we can thus estimate the upper limit of frictional work as 1.2 and 0.6 kJ/mol, respectively, which is roughly 3-4 % of the latent heat.

Since the SCO phenomenon is accompanied by the change of shape and volume of the particles, elastic energy might be stored and released by the sample during the transformation. In a stress-free, high quality single-crystal, this stored elastic energy should be negligible.[71] On the contrary, in polycrystalline samples nucleation takes place in a randomly oriented particle matrix, which is not free from internal stresses. The growth of the nucleated phase will be arrested by grain boundaries and other obstacles within the solid matrix. To overcome the opposing stresses exerted by the surroundings, some additional overcooling/overheating is needed in order to increase the driving force. Because of this 'internal mechanical work', W_e, made by the transforming material, elastic energy will be stored during the forward transition and released in the reverse process. Due to this stored elastic energy, the latent heats of transformation are decreased for both processes. The driving force consumed between the point when the transition starts ($T_{start}^{\mathrm{HS}\rightarrow\mathrm{LS}}$) and ends ($T_{end}^{\mathrm{HS}\rightarrow\mathrm{LS}}$) provides an upper limit to W_e:[67]

$$\Delta G = \frac{1}{2}(T_{end}^{\mathrm{HS}\rightarrow\mathrm{LS}} - T_{start}^{\mathrm{HS}\rightarrow\mathrm{LS}})\Delta S_{SCO} \geq W_e \qquad \text{(Eq. 16)}$$

The corresponding temperature values are tabulated in Tables S10 in the SI and the estimated upper limits of W_e are given in Table 2. The calculated values are rather small, ca. 2 % of the latent heat, indicating that stored elastic energies are negligible in these samples. It should be noted that the actual value of W_e is probably even smaller than this upper limit. In fact, small compositional, structural and microstructural heterogeneities among the powder particles must contribute to the widening of the transition region ($T_{end} - T_{start}$), which limits of course the validity of a quantitative conclusion about the magnitude of W_e. At this point, it is worth to remind also that

ΔG_{chem} is a material property, depending primarily on chemical composition and crystal structure, whereas W_e and W_f are strongly altered by microstructure. Finally, we shall underline that the above considerations refer to constant, atmospheric pressure and implicitly assume that the normal heat capacities of the two phases are equal ($\Delta C_p = {C_p}^{HS} - {C_p}^{LS} = 0$), which is never fully true. Indeed, the excellent cycling reproducibility of the DSC thermograms in our samples allows to assess the exchanged heat in a complete cycle ($\oint dq$), which turns out to be non-zero, the area of the forward transition peak being systematically smaller than that of the reverse transition (see Tables S8-S9). The most likely source of this non-zero value of $\oint dq$ is the heat capacity difference between the two phases:[67]

$$\oint \frac{dq}{T} \approx \Delta C_p \oint \frac{dT}{T} \qquad \text{(Eq. 17)}$$

which allows us to estimate the values of ΔC_p for samples **1** and **2** as ~18 and ~6 J/K.mol, respectively. These values are comparable with the value of 18.7 J/K.mol measured by Sorai and Seki for the compound Fe(1,10-phenanothroline)$_2$(NCS)$_2$ using an adiabatic calorimeter.[63]

4. CONCLUSIONS

In this paper we have assessed some fundamental thermo-elastic properties of two benchmark Fe-triazole SCO complexes. The main findings and prospects are summarized below:

(1) The ordinary thermal expansion was found rather low in both compounds and it was suggested that this might be a general feature in this family of coordination networks.

(2) The transformation strain associated with the SCO is very anisotropic. In line with previous reports,[26-27] the largest expansion occurs along the Fe-triazole chains with values of *ca.* 5 - 6.5 %, similar to other members of the family. This property is crucial for mechanical applications, because it means that different members of this family should provide the same, large amount of

strain – provided the particles can be preferentially oriented. On the contrary, the strain contributions along the other lattice directions are very dissimilar in the two compounds (4 % in **1** and 0 % in **2**) as they depend on intricate details of inter-chain interactions.

(3) The bulk moduli of both compounds are relatively high, with an outstanding 20 GPa value for **1** and 13 GPa for **2**. This property, together with the large strains, must be at the origin of the high cooperativity of the SCO in these compounds. This combination of stiffness and strain provides large elastic potential energies, which could be estimated in **2** as high as 15 J/cm^3 (3 kJ/mol), amounting to *ca.* 15 % of the latent heat. Predictably, the lattice compressibility was found anisotropic, but unexpectedly the Fe-triazole axis turns out to be the most compressible in **1**.

(4) DMA measurements revealed significant elastic softening and associated mechanical losses at the spin transition, which we interpreted as a consequence of the coupling of molecular spin-states to lattice strains. Similar to other types of phase transitions,[52] the strain - spin state coupling coefficients determine the magnitude of changes of the different elastic constants, whereas the shape of these anomalies reflects primarily the order parameter susceptibility. Further work is needed to evaluate the impact(s) of these anelastic phenomena on mechanical applications. To this aim, more quantitative measurements should be conducted in a broad frequency and temperature window on single crystals displaying different SCO behaviors.

(5) Inspired by the vast literature on thermally-induced martensitic transformations,[67] we exploited the very robust calorimetric data of our compounds to quantify different thermo-elastic aspects of the SCO phenomenon, such as the stored elastic energy and the dissipated frictional work. We feel such cross-fertilization of research fields can give rise to interesting comparisons of different classes of phase change materials, both for fundamental and engineering purposes.

ASSOCIATED CONTENT

Supporting Information. The following files are available free of charge. Additional XRD, DMA and DSC data (PDF).

AUTHOR INFORMATION

Corresponding Authors

Gábor Molnár - *LCC, CNRS & University of Toulouse, 205 route de Narbonne, 31077 Toulouse, France*; orcid.org/0000-0001-6032-6393; E-mail: gabor.molnar@lcc-toulouse.fr

Azzedine Bousseksou - *LCC, CNRS & University of Toulouse, 205 route de Narbonne, 31077 Toulouse, France*; E-mail: azzedine.bousseksou@lcc-toulouse.fr

Authors

Damian Paliwoda - LCC, CNRS & University of Toulouse, 205 route de Narbonne, 31077 Toulouse, France

Laure Vendier - LCC, CNRS & University of Toulouse, 205 route de Narbonne, 31077 Toulouse, France

Livia Getzner - LCC, CNRS & University of Toulouse, 205 route de Narbonne, 31077 Toulouse, France

Frederico Alabarse - Elettra Sincrotrone Trieste, S.S. 14 - km 163,5 in AREA Science Park, 34149 Basovizza, Trieste, Italy

Davide Comboni - ESRF, 71 Av. des Martyrs, 38043 Grenoble, France

Baptiste Martin - LCC, CNRS & University of Toulouse, 205 route de Narbonne, 31077 Toulouse, France

Seyed Ehsan Alavi - LCC, CNRS & University of Toulouse, 205 route de Narbonne, 31077 Toulouse, France

Mario Piedrahita Bello - LCC, CNRS & University of Toulouse, 205 route de Narbonne, 31077 Toulouse, France

Lionel Salmon - LCC, CNRS & University of Toulouse, 205 route de Narbonne, 31077 Toulouse, France

William Nicolazzi - LCC, CNRS & University of Toulouse, 205 route de Narbonne, 31077 Toulouse, France

Author Contributions

The manuscript was written through contributions of all authors. All authors have given approval to the final version of the manuscript. Personal contributions include synchrotron XRD experiments (DP, LG, FA, DC), laboratory XRD measurements (LV, DP), DMA and DSC analysis (BM), sample synthesis and characterization (MPB, LS), data curing and theoretical analysis (DP, GM, SEA, LS, WN, AB), writing first draft (DP, GM) and funding acquisition (AB).

Notes

The authors declare no competing financial interest.

ACKNOWLEDGMENTS

This work has received funding from the European Research Council (ERC) under the European Union's Horizon 2020 research and innovation program (grant agreement no. 101019522). The purchase of the SMARTLAB instrument was financed by the PRRI project Nanomat 2020 through the European Regional Development Fund and the Region Occitanie. The high-pressure X-ray

diffraction experiments were performed on the Xpress beamline of the Elettra Sincrotrone Trieste, Italy and at the ID15b beamline of the European Synchrotron Radiation Facility (ESRF), Grenoble, France (Proposal No. CH-6295). The beamtime allocation is gratefully acknowledged. We are indebted to the company Waters Corporation for the loan of the DMA powder sample holder.

REFERENCES

(1) Gütlich, P.; Hauser, A.; Spiering, H. Thermal and optical switching of iron (II) complexes. *Angew. Chem. Int. Ed. Engl.* **1994**, *33*, 2024-2054.

(2) *Spin-crossover materials: properties and applications;* Halcrow, M. A. Ed.; John Wiley & Sons, 2013.

(3) *Spin Crossover in Transition Metal Compounds I-III*; In *Topics Current Chemistry*; Vol. 233-235; Gütlich, P.; Goodwin, H. A. Eds.; Springer, 2004.

(4) Bousseksou, A.; Molnár, G.; Salmon, L.; Nicolazzi, W. Molecular spin crossover phenomenon: recent achievements and prospects. *Chem. Soc. Rev.* **2011**, *40*, 3313-3335.

(5) Kumar, K. S.; Ruben, M. Emerging trends in spin crossover (SCO) based functional materials and devices. *Coord. Chem. Rev.* **2017**, *346*, 176-205.

(6) Molnár, G.; Rat, S.; Salmon, L.; Nicolazzi, W.; Bousseksou, A. Spin crossover nanomaterials: from fundamental concepts to devices, *Adv. Mater.* **2018**, *30*, No. 1703862.

(7) Roubeau, O. Triazole-Based One-Dimensional Spin-Crossover Coordination Polymers. *Eur. J. Inorg. Chem.* **2012**, *18*, 15230-15244.

(8) Lavrenova, L. G.; Shakirova, O. G. Spin crossover and thermochromism of iron(II) coordination compounds with 1,2,4-triazoles and tris (pyrazol-1-yl) methanes. *Eur. J. Inorg. Chem.* **2013**, 670-682.

(9) Kahn, O.; Codjovi, E. Iron (II)-1, 2, 4,-triazole spin transition molecular materials. *Phil. Trans. Royal Soc. A* **1996**, *354*, 359-379.

(10) Garcia, Y.; Niel, V.; Munoz, M. C.; Real, J. A. Spin crossover in 1D, 2D and 3D polymeric Fe (II) networks. *Top. Curr. Chem.* **2004**, *233*, 229-257.

(11) Lavrenova, L. G.; Larionov, S. V. Spin transition in iron(II) complexes with 1,2,4-triazoles and tetrazoles. *Russian J. Coord. Chem.* **1998**, *24*, 379-395.

(12) Koningsbruggen, P. J. V. Special classes of iron (II) azole spin crossover compounds. *Top. Curr. Chem.* **2004**, *233*, 123-149.

(13) Enríquez-Cabrera, A.; Routaboul, L.; Salmon, L.; Bousseksou, A. Complete post-synthetic modification of a spin crossover complex. *Dalton Trans.* **2019**, *48*, 16853-16856.

(14) Haasnoot, J. G.; Vos, G.; Groeneveld, W. L. 1,2,4-Triazole Complexes, III. Complexes of Transition Metal(II) Nitrates and Fluoroborates. *Z. Naturforsch. B* **1977**, *32*, 1421-1430.

(15) Lavrenova, L. G.; Ikorskii, V. N.; Varnek, V. A.; Oglezneva, I. M.; Larionov, S. V. High-temperature spin transition in coordination compounds of iron (II) with triazoles (in Russian). *Sov. J. Coordinat. Chem.* **1986**, *12*, 207-215.

(16) Kröber, J.; Audière, J. P.; Claude, R.; Codjovi, E.; Kahn, O.; Haasnoot, J. G.; Grolière, F.; Jay, C.; Bousseksou, A.; Linarès, J.; Varret, F.; Gonthier-Vassal, A. Spin Transitions and Thermal Hysteresis in the Molecular-Based Materials $[Fe(Htrz)_2(trz)](BF_4)$ and $[Fe(Htrz)_3](BF_4)_2 \cdot H_2O$ (Htrz = 1,2,4-4H-triazole; trz = 1,2,4-triazolato). *Chem. Mater.* **1994**, *6*, 1404-1412.

(17) Sugiyarto, K. H.; Goodwin, H. A. Cooperative Spin Transitions in Iron(II) Derivatives of 1,2,4-Triazole. *Aust. J. Chem.* **1994**, *47*, 263– 277.

(18) Roubeau, O.; Haasnoot, J. G.; Codjovi, E.; Varret, F.; Reedijk, J. Spin Transition Regime in New One-Dimensional Polymeric Iron(II) Compounds. Importance of the Water Content for the Thermal and Optical Properties. *Chem. Mater.* **2002**, *14,* 2559–2566.

(19) Kahn, O.; Kröber, J.; Jay, C. Spin transition molecular materials for displays and data recording. *Adv. Mater.* **1992**, *4*, 718-728.

(20) Kahn, O.; Martinez, C. J. Spin-transition polymers: from molecular materials toward memory devices. *Science* **1998**, *279*, 44-48.

(21) Sheludyakova, L. A.; Lavrenova. L. G. IR spectral study of the 1A1⇄5T2 spin transition in Iron(II) complexes with 1,2,4-triazole. *J. Struct. Chem.* **1997**, *38*, 853-856.

(22) Michalowicz, A.; Moscovici, J.; Ducourant, B.; Cracco, D.; Kahn, O. EXAFS and X-ray powder diffraction studies of the spin transition molecular materials $[Fe(Htrz)_2(trz)](BF_4)$ and $[Fe(Htrz)_3](BF_4)_2.H_2O$ (Htrz=1,2,4-4H-triazole; trz=1,2,4-triazolato). *Chem. Mater.* **1995**, *7*, 1833-1842.

(23) Verelst, M.; Sommier, L.; Lecante, P.; Mosset, A.; Kahn, O. Structural Study by Wide-Angle X-ray Scattering of the Spin Transition Molecular Materials $[Fe(Htrz)_2(trz)](BF_4)$ and

[$Fe(NH_2trz)_3](NO_3)_2$ (Htrz=1,2,4-4H-Triazole, trz=1,2,4-Triazolato). *Chem. Mater.* **1998**, *10*, 980-985.

(24) Haasnoot, J. G. Mononuclear, oligonuclear and polynuclear metal coordination compounds with 1,2,4-triazole derivatives as ligands. *Coord. Chem. Rev.* **2000**, *200*, 131-185.

(25) Grosjean, A.; Daro, N.; Kauffmann, B.; Kaiba, A.; Létard, J.-F.; Guionneau, P. The 1-D polymeric structure of the $[Fe(NH_2trz)_3](NO_3)_2 \cdot nH_2O$ (with n= 2) spin crossover compound proven by single crystal investigations. *Chem. Commun.* **2011**, *47*, 12382-12384.

(26) Grosjean, A. Matériaux polymériques 1D à transition de spin : investigations structurales multi-échelles. Ph.D. Dissertation, University of Bordeaux, Bordeaux, France, 2013.

(27) Grosjean, A.; Négrier, P.; Bordet, P.; Etrillard, C.; Mondieig, D.; Pechev, S.; Lebraud, E.; Létard, J.-F.; Guionneau, P. Crystal Structures and Spin Crossover in the Polymeric Material $[Fe(Htrz)_2(trz)](BF_4)$ Including Coherent-Domain Size Reduction Effects. *Eur. J. Inorg. Chem.* **2013**, 796-802.

(28) Sirenko, V. Y.; Kucheriv, O. I.; Rotaru, A.; Fritsky, I. O.; Gural'skiy, I. Y. A.; Direct Synthesis of Spin-Crossover Complexes: An Unexpectedly Revealed New Iron-Triazolic Structure. *Eur. J. Inorg. Chem.* **2020**, 4523-4531.

(29) Nieto Castro, D. Advances in Spin Crossover: Synthesis, Mechanosynthesis and Switchable Multifunctional Hybrids, Ph.D. Dissertation, Universitat Rovira i Virgili, Tarragona, Spain, 2021.

(30) Spiering, H.; Meissner, E.; Köppen, H.; Müller, E. W.; Gütlich, P. The effect of the lattice expansion on high spin⇌ low spin transitions. *Chem. Phys.* **1982**, *68*, 65-71.

(31) Spiering, H. Elastic interaction in spin-crossover compounds. *Top. Curr. Chem.* **2004**, *235*, 171-195.

(32) Shepherd, H. J.; Gural'skiy, I. Y. A.; Quintero, C. M.; Tricard, S.; Salmon, L.; Molnár, G.; Bousseksou, A. Molecular actuators driven by cooperative spin-state switching. *Nat. Commun.* **2013**, *4*, No. 2607.

(33) Koo, Y. S.; Galán-Mascarós, J. R. Spin crossover probes confer multistability to organic conducting polymers. *Adv. Mater.* **2014**, *26*, 6785-6789.

(34) Rat, S.; Piedrahita-Bello, M.; Salmon, L.; Molnár, G.; Demont, P.; Bousseksou, A. Coupling mechanical and electrical properties in spin crossover polymer composites. *Adv. Mater.* **2018**, *30*, No. 1705275.

(35) Piedrahita-Bello, M.; Angulo-Cervera, J. E.; Courson, R.; Molnár, G.; Malaquin, L.; Thibault, C.; Tondu, B.; Salmon, L.; Bousseksou, A. 4D printing with spin-crossover polymer composites. *J. Mater. Chem. C* **2020**, *8*, 6001-6005.

(36) Suleimanov, I.; Costa, J. S.; Molnár, G.; Salmon, L.; Fritsky, I.; Bousseksou, A. Effect of ligand substitution in $[Fe(H\text{-}trz)_2(trz)]BF_4$ spin crossover nanoparticles. *French-Ukrainian J. Chem.* **2015**, *3*, 66-72.

(37) Tateiwa, N.; Haga, Y. Evaluations of pressure-transmitting media for cryogenic experiments with diamond anvil cell. *Rev. Sci. Instr.* **2009**, *80*, No. 123901.

(38) Piermarini, G. J.; Block, S.; Barnett, J. D.; Forman, R. A. Calibration of the pressure dependence of the R 1 ruby fluorescence line to 195 kbar. *J. Appl. Phys.* **1975**, *46*, 2774-2780.

(39) Prescher, C.; Prakapenka, V. B. DIOPTAS: a program for reduction of two-dimensional X-ray diffraction data and data exploration. *High Press. Res.* **2015**, *35*, 223–230.

(40) LeBail, A. Whole Powder Pattern Decomposition Methods and Applications: A Retrospection. *Powder Diffr.* **2005**, *20*, 316-326.

(41) Petricek, V.; Dusek, M.; Palatinus, L. Crystallographic Computing System JANA2006: General features. *Z. Kristallogr.* **2014**, *229*, 345-352.

(42) Mahlin, D.; Wood, J.; Hawkins, N.; Mahey, J.; Royall, P. G. A novel powder sample holder for the determination of glass transition temperatures by DMA. *Inter. J. Pharm.* **2009**, *371*, 120–125.

(43) Miller, W.; Smith, C. W.; Mackenzie, D. S.; Evans, K. E. Negative thermal expansion: a review. *J. Mater. Sci.* **2009**, *44*, 5441-5451.

(44) Angel, R. J. Equations of State. *Rev. Mineral. Geochem.* **2001**, *41*, 35-59.

(45) Mikolasek, M.; Manrique-Juarez, M. D.; Shepherd, H. J.; Ridier, K.; Rat, S.; Shalabaeva, V.; Bas, A.-C.; Collings, I. E.; Mathieu, F.; Cacheux, J.; Leichle, T.; Nicu, L.; Nicolazzi, W.; Salmon, L.; Molnar, G.; Bousseksou, A. Complete Set of Elastic Moduli of a Spin-Crossover Solid: Spin-State Dependence and Mechanical Actuation. *J. Am. Chem. Soc.* **2018**, *140*, 8970–8979.

(46) Pinheiro, A.; Mano, J. F. Study of the glass transition on viscous-forming and powder materials using dynamic mechanical analysis. *Polymer Testing* **2009**, *28*, 89-95.

(47) Kissi, E. O.; Grohganz, H.; Löbmann, K.; Ruggiero, M. T.; Zeitler, J. A.; Rades, T. Glass-Transition Temperature of the β-Relaxation as the Major Predictive Parameter for Recrystallization of Neat Amorphous Drugs. *J. Phys. Chem. B* **2018**, *122*, 2803–2808

(48) Xiao, M.; Sadhanala, A.; Abdi-Jalebi, M.; Thomas, T. H.; Ren, X.; Zhang, T.; Chen, H.; Carey, R. L.; Wang, Q.; Senanayak, S. P.; Jellett, C.; Onwubiko, A.; Moser, M.; Liao, H.; Yue, W.; McCulloch, I.; Nikolka, M.; Sirringhaus, H. Linking Glass-Transition Behavior to Photophysical and Charge Transport Properties of High-Mobility Conjugated Polymers. *Adv. Funct. Mater.* **2021**, *31*, No. 2007359.

(49) Pérez-Sáez, R. B.; Recarte, V.; Nó, M. L.; San Juan, J. Anelastic contributions and transformed volume fraction during thermoelastic martensitic transformations. *Phys. Rev. B* **1998**, *57*, 5684-5692.

(50) Jackson, I. Properties of rocks and minerals: physical origins of anelasticity and attenuation in rock. *Treatise on Geophys.* **2015**, *2*, 539-571.

(51) Rat, S.; Nagy, V.; Suleimanov, I.; Molnar, G.; Salmon, L.; Demont, P.; Csoka, L.; Bousseksou, A. Elastic coupling between spin-crossover particles and cellulose fibers. *Chem. Commun.* **2016**, *52*, 11267-11269.

(52) Carpenter, M. A.; Salje, E. K. Elastic anomalies in minerals due to structural phase transitions. *Eur. J. Mineral.* **1998**, 693-812.

(53) Mason, H. E.; Li, W.; Carpenter, M. A.; Hamilton, M. L.; Howard, J. A.; Sparkes, H. A. Structural and spectroscopic characterisation of the spin crossover in $[Fe(abpt)_2(NCS)_2]$ polymorph A. *New J. Chem.* **2016**, *40*, 2466-2478.

(54) Jakobsen, V. B.; Trzop, E.; Dobbelaar, E.; Gavin, L. C.; Chikara, S.; Ding, X.; Lee, M.; Esien, K.; Müller-Bunz, H.; Felton, S.; Collet, E.; Carpenter, M. A.; Zapf, V. S.; Morgan, G. G. Domain Wall Dynamics in a Ferroelastic Spin Crossover Complex with Giant Magnetoelectric Coupling. *J. Am. Chem. Soc.* **2021**, *144*, 195–211.

(55) Dobbelaar, E.; Jakobsen, V. B.; Trzop, E.; Lee, M.; Chikara, S.; Ding, X.; Müller-Bunz, H.; Esien, K.; Felton, S.; Carpenter, M. A.; Collet, E.; Morgan, G. G.; Zapf, V. S. Thermal and Magnetic Field Switching in a Two-Step Hysteretic MnIII Spin Crossover Compound Coupled to Symmetry Breakings. *Angew. Chem. Int. Ed.* **2022**, *61*, No. e202114021.

(56) Wu, Z.; Justo, J. F.; Da Silva, C. R. S.; De Gironcoli, S.; Wentzcovitch, R. M. Anomalous thermodynamic properties in ferropericlase throughout its spin crossover. *Phys. Rev. B* **2009**, *80*, No. 014409.

(57) Nowick, A. S.; Berry, B. S. *Anelastic relaxation in crystalline solids*; Academic Press, 1972.

(58) Manrique-Juarez, M. D.; Mathieu, F.; Shalabaeva, V.; Cacheux, J.; Rat, S.; Nicu, L.; Leichlé, T.; Salmon, L.; Molnar, G.; Bousseksou, A. A Bistable Microelectromechanical System Actuated by Spin-Crossover Molecules. *Angew. Chem. Int. Ed.* **2017**, *129*, 8186-8190.

(59) Carpenter, M. A.; Zhang, Z. Anelasticity maps for acoustic dissipation associated with phase transitions in minerals. *Geophys. J. Internat.* **2011**, *186*, 279-295.

(60) Chernyshov, D.; Bürgi, H. B.; Hostettler, M.; Törnroos, K. W. Landau theory for spin transition and ordering phenomena in Fe (II) compounds. *Phys. Rev. B* **2004**, *70*, No. 094116.

(61) Azzolina, G.; Bertoni, R.; Collet, E. General Landau theory of non-symmetry-breaking and symmetry-breaking spin transition materials. *J. Appl. Phys.* **2021**, *129*, No. 085106.

(62) Collet, E.; Azzolina, G. Coupling and decoupling of spin crossover and ferroelastic distortion: Unsymmetric hysteresis loop, phase diagram, and sequence of phases. *Phys. Rev. Mater.* **2021**, *5*, No. 044401.

(63) Sorai, M.; Seki, S. Phonon coupled cooperative low-spin $^{1}A_{1}$ high-spin $^{5}T_{2}$ transition in $[Fe(phen)_2(NCS)_2]$ and $[Fe(phen)_2(NCSe)_2]$ crystals. *J. Phys. Chem. Solids* **1974**, *35*, 555-570.

(64) Sorai, M. Heat capacity studies of spin crossover systems. *Top. Curr. Chem.* **2004**, *235*, 153-170.

(65) Bousseksou, A.; McGarvey, J. J.; Varret, F.; Real, J. A.; Tuchagues, J. P.; Dennis, A. C.; Boillot, M. L. Raman spectroscopy of the high-and low-spin states of the spin crossover complex $Fe(phen)_2(NCS)_2$: an initial approach to estimation of vibrational contributions to the associated entropy change. *Chem. Phys. Lett.* **2000**, *318*, 409-416.

(66) Molnár, G.; Mikolasek, M.; Ridier, K.; Fahs, A.; Nicolazzi, W.; Bousseksou, A. Molecular spin crossover materials: Review of the lattice dynamical properties. *Annal. Phys.* **2019**, *531*, No. 1900076.

(67) Wollants, P.; Roos, J. R.; Delaey, L. Thermally-and stress-induced thermoelastic martensitic transformations in the reference frame of equilibrium thermodynamics. *Prog. Mater. Sci.* **1993**, *37*, 227-288.

(68) Torra, V.; Tachoire, H. Martensitic transformations in shape-memory alloys: successes and failures of thermal analysis and calorimetry. *Thermochim. Acta* **1992**, *203*, 419-444.

(69) Yawny, A.; Lovey, F. C.; Torra, V. Entropy production in single-crystal single-interface martensite transformation. *Scripta Metallurg. Mater.* **1995**, *32*, 439-444.

(70) Isola, L. M.; Malvasio, B. F.; Giordana, M. F.; Malarria, J. Effect of the precipitates on the thermodynamics of the martensitic transformations in Ti-rich Ni-Ti-Co thin films. *J. Alloys Comp.* **2020**, *818*, No. 152904.

(71) Beke, D. L.; Daróczi, L.; Elrasasi, T. Y. Determination of elastic and dissipative energy contributions to martensitic phase transformation in shape memory alloys. In *Shape Memory Alloys-Processing, Characterization and Applications*; Fernandes, F. M. B. Ed.; IntechOpen, 2013, pp. 167-196.

FOR TABLE OF CONTENTS USE ONLY

On the Elastic Properties of the Iron(II)-Triazole Spin Crossover Complexes $[Fe(Htrz)_2trz]BF_4$ and $[Fe(NH_2trz)_3]SO_4$

Damian Paliwoda, Laure Vendier, Livia Getzner, Frederico Alabarse, Davide Comboni, Baptiste Martin, Seyed Ehsan Alavi, Mario Piedrahita Bello, Lionel Salmon, William Nicolazzi, Gábor Molnár,* Azzedine Bousseksou*

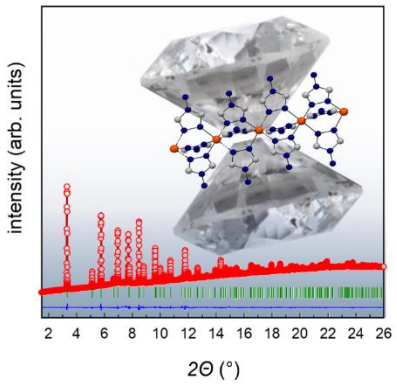

The transformation strain, the compressibility and calorimetric properties are assessed for two benchmark Fe(II)-triazole spin-crossover compounds. Considerable elastic softening and mechanical damping are revealed in both compounds at the spin transition. The knowledge of these properties helps understanding the spin crossover mechanism and guides the development of spin crossover based mechanical transducers.